Journal of Catalysis 372 (2019) 352–361

Contents lists available at ScienceDirect

Journal of Catalysis

journal homepage: www.elsevier.com/locate/jcat

Regioselective oxidative carbon-oxygen bond cleavage catalysed by copper(II) complexes: A relevant model study for lytic polysaccharides monooxygenases activity

Sethuraman Muthuramalingam [a], Duraiyarasu Maheshwaran [a], Marappan Velusamy [b], Ramasamy Mayilmurugan [a,*]

[a] Bioinorganic Chemistry Laboratory/Physical Chemistry, School of Chemistry, Madurai Kamaraj University, Madurai 625021, Tamilnadu, India
[b] Department of Chemistry, North Eastern Hill University, Shillong 793022, India

ARTICLE INFO

Article history:
Received 14 November 2018
Revised 8 March 2019
Accepted 13 March 2019

Keywords:
Lytic polysaccharides monooxygenases
Copper(II) model complexes
Oxidative cleavage
Reaction mechanism

ABSTRACT

Lytic polysaccharide monooxygenases (LPMOs) are copper-containing monooxygenase and catalyzing the oxidative cleavage of recalcitrant polysaccharides using dioxygen. The copper(II) complexes [Cu(L1)(H_2O)ClO_4]ClO_4 **1**, [L1 = 4-methyl-1-[(pyridin-2-yl-methyl)]-1,4-diazepane]; [Cu(L2)(H_2O)ClO_4]ClO_4 **2**, [L2 = 4-methyl-1-[(2-(pyridine-2-yl)ethyl]-1,4-diazepane] and [Cu(L3)(H_2O)ClO_4]ClO_4 **3**, [L3 = 1-(4-methoxy-3,5-dimethyl-pyridin-2-yl)methyl)-4-methyl-1,4-diazepane] have been synthesized and characterized as the novel models for LPMOs. The molecular structures exhibit distorted square pyramidal geometry (τ, 0.183–0.388) as similar to LPMOs. The Cu—N (1.99–2.02 Å) bond distances of the model complexes are almost identical to those of native LPMOs enzyme (1.9–2.2 Å). The 1, 4-diazepane backbone and pyridine unit of complexes provide reasonable structural resemblances to 'histidine brace' and histidine residues of LPMOs respectively. The spectral, redox and kinetic studies were performed in water to mimic accurate enzymatic reaction conditions. The well-defined Cu(II)/Cu(I) reduction couples were observed around 8–112 mV versus NHE, which is lower than that of LPMOs. The electronic spectra of the complexes showed the d-d transitions around 600–635 nm and axial EPR parameter ($g_{||}$, 2.28–2.29; $A_{||}$, 160–168 × 10^{-4} cm^{-1}), which are almost identical to that of LPMOs. The model complexes were catalyzed oxidative cleavage of model substrate *p*-nitrophenyl-*β*-D-glucopyranoside into *p*-nitrophenol and D-allose with a maximum yield up to 78.4% and TON, 300. The kinetics of reaction monitored by following the formation of an absorption band around at 400 nm corresponds to *p*-nitrophenol, showed the rate of 3.19–5.26 × 10^{-3} s^{-1}. The oxidative cleavage reaction may occur via Cu^{II}-OOH intermediate, whose formation accompanied by an electronic spectral signature around 375 nm with the rate of 1.61–9.06 × 10^{-3} s^{-1}. The Cu^{II}-OOH intermediate was characterized by spectral methods and its geometry was optimized by DFT calculations.

1. Introduction

The sustainable production of energy and materials from biomass is of global importance and crucial to establish a sustainable bio-based economy [1,2]. The enzymatic catalytic conversion of inert lignocellulosic biomass into fuels was revolutionized by the discovery of lytic polysaccharide monooxygenases (LPMOs) that perform oxidative cleavage of recalcitrant polysaccharides such as cellulose, chitin, etc [3–8]. The LPMOs are mononuclear copper-containing enzymes and are isolated from cellulolytic fungi and actinomycete bacteria [9–11]. It has an unusual surface-exposed active site with a tightly bound Cu(II) ion that catalyzes the regioselective hydroxylation of crystalline cellulose, leading to glycosidic bond cleavage (Scheme 1). The active site of LPMOs structures exhibited square pyramidal/pseudo-octahedral geometry constituted by three nitrogens of two histidine residues (His 86 and His 19), of which one is coordinated via N-terminal motif and termed as the 'histidine brace' and two water molecules complete the square pyramidal geometry [8–11]. The LPMOs catalyzes the scission of a polysaccharide chain by activating glycosidic C—H bond using molecular oxygen (Scheme 1). It performs oxidative cleavage of C1 and C4 positions at reducing and oxidation ends respectively [3–5].

* Corresponding author.
E-mail address: mayilmurugan.chem@mkuniversity.org (R. Mayilmurugan).

https://doi.org/10.1016/j.jcat.2019.03.019
0021-9517/

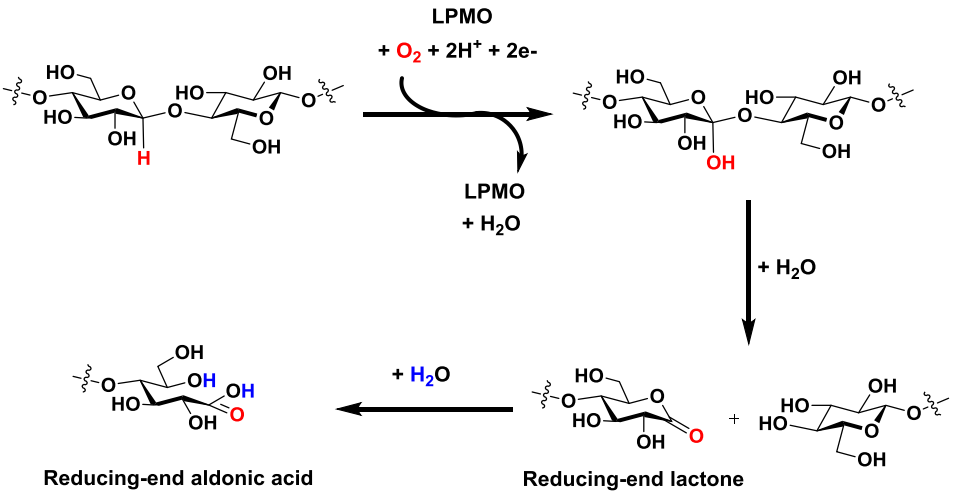

Scheme 1. Enzymatic oxidative cleavage of a polysaccharide chain by LPMOs using O_2.

Despite several elegant biochemical reports available for the LPMOs but only two biomimetic model studies are known to date. Castillo and co-workers reported the first structural model of copper(II) complexes based on the bis(benzimidazole)amine ligand in 2014, but no reactivity was performed [12]. Recently, Simaan and co-workers reported another bioinspired copper(II) complexes as a functional model for LPMOs. The model oxidative cleavages reactions were studied using *p*-nitrophenyl-β-D-glucopyranoside as substrate and H_2O_2 as an oxygen source, where a maximum turn over number (TON) of 50 was achieved [13]. In which, the reaction postulated to proceed via reactive copper-oxygen species and hydroxylate selectively strong C—H bond [14]. It is similar to the report of Itoh and co-workers, where copper(II)-superoxide intermediate is proposed for the aliphatic C—H activation [15]. Whereas, Tolman and co-workers have proposed more reactive $[CuOH]^{2+}$ species for activating C—H bonds of the polysaccharide [16]. In fact, the LPMOs mechanism is not well understood until today. Particularly, an open question remains unanswered stage: whether the oxidative cleavage of proceeds via Cu(II)-OOH/Cu(II)-OO· or $[CuOH]^{2+}$ species. The design and synthesis of bioinspired models are essential for further better understanding of this mechanism. In this article, we report synthesize and characterization of 1, 4-diazepane based 3 N ligand systems and their copper(II) complexes, which exhibits very close chemical and structural arrangements to the active site geometry of LPMO enzyme. The 1, 4-diazepane backbone and pyridine units exhibit approximate structural similarities to 'histidine brace' and histidine residues of LPMOs respectively. Our model systems adopt identical square pyramidal geometry to duly duplicate the coordination environment of LPMOs. They catalyze the oxidative cleavage of the model substrate *p*-nitrophenyl-*β*-D-glucopyranoside in water. Interestingly, spectral, redox and kinetic studies were performed in water to mimic accurate enzymatic reaction conditions. The present of 1, 4-diazepane architecture and additional pyridine nitrogen donor property of ligands provide important differences to other previously reported catalysts and the catalytic performances. Our design and synthesis is a novel example of structural and functionally relevant biomimetic models for LPMOs. Thus, the present copper(II) complexes exhibit very similar chemical surroundings as in the active site of LPMOs and mimic its function elegantly.

2. Results and discussion

The methyl-substituted cyclic 1, 4-diazepane has been used as the starting material and its amino hydrogen was substituted by pyridylmethyl, pyridylethyl, and 4-methoxy-3,5-dimethyl pyridyl moieties to synthesize the ligands. The ligands L1 - L3 were synthesized from the known synthetic methodology [17–22], which involve substitution and condensation reactions. The ligand L1 and L3 have been synthesized by a simple substitution reaction of one equivalent of 1-methyl homopiperazine with 2-picolylchloride hydrochloride and 2-chloromethyl-4-methoxy-3,5-dimethylpyridine hydrochloride respectively. The ligand L2 was synthesized by condensation reaction of 2-vinylpyridine and 1-methyl homopiperazine under acidic condition. The copper(II) complexes $[Cu(L1)(H_2O)ClO_4]ClO_4$ **1**, $[Cu(L2)(H_2O)ClO_4]ClO_4$ **2** and $[Cu(L3)(H_2O)ClO_4]ClO_4$ **3** (Scheme 2) have been isolated as dark blue colour crystalline solids by the reaction of corresponding ligand with copper(II) perchlorate in methanol:H_2O (8:2) mixture. The formation of the complexes was confirmed by elemental analysis and ESI-MS in acetonitrile showed the predominant peaks at *m/z* values of 368.18, 399.20 and 427.25 corresponding to $[Cu(L1)ClO_4]^+$, $[Cu(L2)(H_2O)ClO_4]^+$, and $[Cu(L3)ClO_4]^+$ respectively (Figs. S1 –S3). The formation of complexes was further supported by single crystal X-ray structures of **1** and **2**.

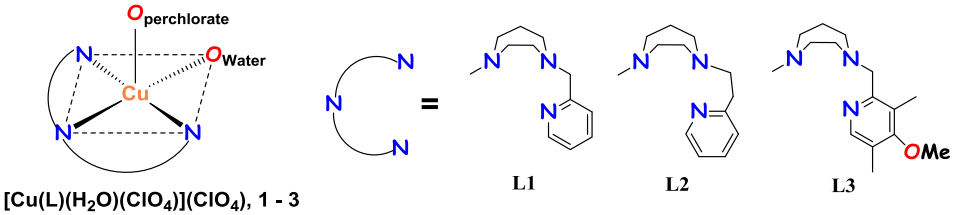

$[Cu(L)(H_2O)(ClO_4)](ClO_4)$, 1 - 3

Scheme 2. Structure of copper(II) complexes and ligands used in the present study.

2.1. Molecular structures of *1* and *2*

The single crystal X-ray crystallographic data of the copper(II) complexes **1** and **2** together with selected bond lengths and angles and structure refinement parameters are summarized in Tables 1. and S4. The molecular structures of **1** and **2** exhibit monomeric complex unit (Fig. 1) with the distorted square pyramidal geometry as revealed from τ value of 0.183 and 0.388 respectively [τ = (β − α)/60; β (O1-Cu1-N2) and α (N1-Cu1-N3); for perfect square pyramidal and trigonal-bipyramidal geometries, τ = 0 and 1 respectively] [23]. The geometrical distortion is slightly lower in **1** than **2,** but higher than previously reported 1,4-diazepane based CuN4 complexes (τ, 0.064, 0.125) [24]. The copper(II) center is coordinated to two tertiary amine nitrogen atoms, one pyridyl nitrogen atom and one oxygen atom of water molecules, which constitute the basal plane of the square pyramid. The oxygen atom of perchlorate (ClO_4^-) anion occupies the apical site of the square pyramid. The observed Cu—O_{water} bond distance of **1** (1.953 Å) is shorter than that of **2** (2.035 Å) and these bond distances are shorter than Cu—$O_{perchlorate}$ bonds (**1**, 2.428; **2**, 2.377 Å). Further, the equatorial Cu—O_{water} bond distances of **1** and **2** are shorter than that of LPMOs enzymes (Cu—O_{water}, 2.2 Å). Also, the axial Cu—O bond distances are shorter than Cu—O_{water} bond distance of LPMOs enzymes (Cu—O_{water}, 2.8 Å). The axial elongation of Cu—$O_{perchlorate}$ is due to the John Teller distortion and this counter ion is highly labile, can be replaced by water molecules in solution. The Cu—N_{Py} (1.989 Å) bond distance of **1** is slightly shorter than Cu—N_{amine} (1.994, 2.006 Å) bond distances, which are slightly shorter than those of **2** (Cu—N_{Py}, 1.994 Å; Cu—N_{amine}, 2.019, 2.022 Å). The Cu-N bond distances are almost similar to the Cu—N bond distances of the native LPMOs enzyme (Cu—$N_{His\text{-}1}$, 1.9 Å, Cu—$N_{His\text{-}78}$, 2.1 Å, and Cu—NH_2, 2.2 Å). The bond angles of O(1)—Cu—N(2) (**1**, 173.57°; **2**, 153.38°) and N(1)-Cu(1)-N(3) (**1**, 162.58°; **2**, 174.65°) are lower than the normal square pyramidal geometry (180°). The bond angles O(1)—Cu(1)—N(1) (**1**, 95.06°; **2**, 92.17°), O(1)-Cu(1)-N(3) (**1**, 99.44°; **2**, 92.37°) are higher than the expected value for square pyramidal geometry (90°) and the other bond angles N(2)—Cu(1)—N(3) (**1**, 80.79°; **2**, 80.33). The steric nature of ligands unable to place all the nitrogen atoms and copper(II) center in the same square plane. The structural similarity of model complex and enzyme is visualized by the superposition of **1** on the active site structure of LPMOs (Fig. 1). The main difference between the two geometries is the torsion around the Cu-N axes, enforced by the rigidity of the sterically constrained ligand structure of our model system.

Table 1
Selected bond lengths[a] [Å] and bond angles[a] [°] for **1** and **2.**

	1	2
Cu(1)—O(1)	1.953(3)	2.035(3)
Cu(1)—N(1)	1.989(3)	1.994(3)
Cu(1)—N(2)	1.994(3)	2.019(3)
Cu(1)—N(3)	2.006(3)	2.022(3)
Cu(1)—O(2)	2.428(4)	2.377(3)
O(1)—Cu(1)—N(1)	95.06(13)	92.17(12)
O(1)—Cu(1)—N(2)	173.57(12)	151.38(12)
N(1)—Cu(1)—N(2)	83.73(13)	96.94(13)
O(1)—Cu(1)—N(3)	99.44(14)	92.37(13)
N(1)—Cu(1)—N(3)	162.58(14)	174.65(13)
N(2)—Cu(1)—N(3)	80.79(14)	80.33(13)
O(1)—Cu(1)—O(2)	96.87(12)	93.86(12)
N(1)—Cu(1)—O(2)	87.65(14)	88.25(12)
N(2)—Cu(1)—O(2)	89.40(12)	113.42(13)
N(3)—Cu(1)—O(2)	100.08(15)	88.63(12)

[a] Standard deviations in parenthesis.

2.2. Electronic spectra

The absorption spectra of **1**–**3** showed two major absorption bands in the range of 261–265 nm and 600–635 nm in water, which are corresponding to intra-ligand π-π* and d-d transitions respectively (Fig. 2a, Table 2) [25–27]. The energy of transitions

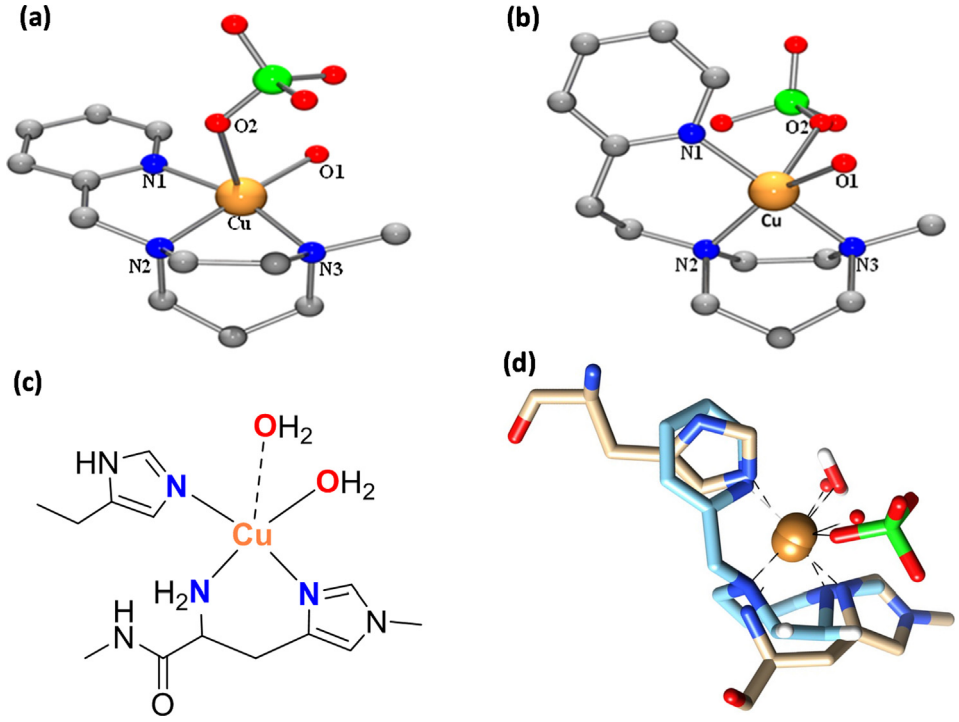

Fig. 1. (a) The molecular structure of **1** (a) and **2** (b) (Pov-ray figures drawn from 50% probability factor of thermal ellipsoids). The hydrogen atoms and ClO_4^- ions are omitted for clarity. (c) Active site structure of LPMO. (d) Overlay of the active site structure of LPMO from *thermoascus auriantacus* to **1**.

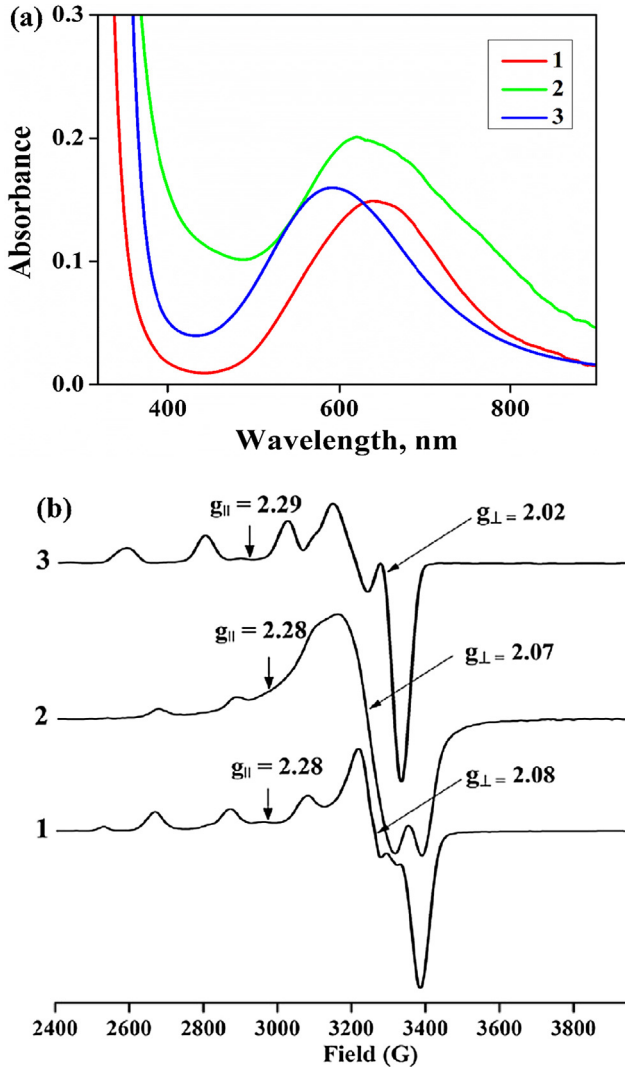

Fig. 2. (a) Electronic absorption spectra of complexes **1–3** in H_2O (1×10^{-3} M) at 25 °C. (b) EPR spectra for **1–3** in methanol: DMF (8:2) at 70 K.

is not affected by ligand architecture but their intensity significantly varied. The position of d-d transitions around 600–635 nm supports the existence of square pyramidal geometry around copper(II) coordination sphere with the d^2_{x-y} ground state [28,29]. The energies of the d-d transition of model complexes are very close to the LPMOs (655 nm) [30]. However, they are slightly higher than those of analogous CuN4 complexes of 1,4-diazepane based ligands [24] and revealing that lower geometrical distortion [31–35].

The EPR spectra of **1–3** were found be anisotropic in methanol: DMF (8:2) mixture at 70 K and their hyperfine features have been resolved into parallel ($g_{||}$) regions. But the perpendicular ($g_{\perp}$) regions were appeared as intense and unresolved signals due to the Zeeman splitting of the ground state doublet along the z-axis of the complexes (Fig. 2b, Table 2). The axial EPR spectra of **1–3** with $g_{||}$, 2.25–2.37 > $g_{\perp}$, 2.02–2.08 suggesting the presence of $^1B_{2g}$ ground state with the unpaired electron on $d^2_{x-y}{}^2$ orbital [36,37]. The minor g-components appeared at 2.32 and 2.19 for **1** and 2.41, 2.21 and 2.13 for **3**, are corresponding to the additional species formed in solution. They are possibly originated from solvation that resulted in water exchange with the anion or deprotonation [38]. The highest-energy half-occupied d-orbital being $d^2_{x-y}{}^2$ and its lobes pointing to the ligand orbitals with largest repulsive or antibonding interaction with the ligand field [39,40]. The complexes exhibit $g_{||} > g_{\perp}$ with *f*-values of the range 135–145 cm^{-1} and are close to the range of the square-based geometries (105–135 cm^{-1}) [41]. The larger $A_{\perp}$ values (141–153 $\times 10^{-4}$ cm^{-1}) is further supporting the existence of square pyramidal geometries for **1–3**. The complex **1** shows a larger hyperfine splitting in the g_z region with $A_{||}$ value of 176 $\times 10^{-4}$ cm^{-1} which is higher than that of **2** ($A_{||}$, 156 $\times 10^{-4}$ cm^{-1}) and **3** ($A_{||}$, 157 $\times 10^{-4}$ cm^{-1}). However, the $A_{||}$ value range of 156–176 $\times 10^{-4}$ cm^{-1} suggesting the presence of D_{4h} symmetry [42]. This hyperfine coupling $A_{||}$ of the unpaired electron to the nuclear spin of the copper(II) centre is possibly contributed from lower Fermi contact, spin dipolar and orbital dipolar [43]. The larger g and lower *A* values suggest the existence of axial ligand coordination and more delocalization of charge into the ligand orbitals due to the formation of square pyramidal structure [20]. The g values are not significantly affected by ligand architecture but expressively higher $A_{||}$ and $A_{\perp}$ values have been obtained for **1** than those of **2** and **3**. Interestingly, the present complexes exhibit very similar EPR parameters to the LPMOs ($g_{||}$ = 2.23 – 2.28; $g_{\perp}$ = 2.06 – 2.09). The $A_{||}$ values of **2** (156 $\times 10^{-4}$ cm^{-1}) and **3** (157 $\times 10^{-4}$ cm^{-1}) are almost identical to LPMOs (147–156 $\times 10^{-4}$ cm^{-1}) [3-5,30], which are lower than that of observed for **1** (176 $\times 10^{-4}$ cm^{-1}).

The EPR parameters and the energy of d-d transition were used to estimate bonding parameters such as covalency of in-plane σ-bonds (α^2), in-plane π-bonds (β^2) and out-plane π-bonds (γ^2) [44]. The complexes exhibited α^2 (**1**, 0.929; **2**, 0.780; **3**, 0.731), β^2 (**1**, 1.005; **2**, 1.046; **3**, 1.045) and γ^2 (**1**, 0.924; **2**, 1.032; **3**, 0.558)

Table 2
Electronic spectral and redox data for **1–3** in water.

Complex	Electronic Spectra[a] λ_{max}, nm (ε, M^{-1} cm^{-1})	EPR parameters[b]										Redox Data[c]				
		$g_{||}$	$g_{\perp}$	$A_{||}$	$A_{\perp}$	*f* (cm)	α^2	β^2	γ^2	$K_{||}$	$K_{\perp}$	Ep_a (V)	Ep_c (V)	ΔE (mV)	$E_{1/2}$ (V) (vs. Ag/Ag^+)	$E_{1/2}$ (V) (vs. NHE)
1	635 (139), 261(15490), 290 (7060)	2.28	2.08	168	154	136	0.818	0.993	0.902	0.813	0.738	−0.140 -	−0.285 −0.269[d]	145	−0.213	0.008
2	630 (199), 265 (23580), 293 (12780)	2.28	2.07	163	149	148	0.799	1.020	0.812	0.816	0.649	−0.165 -	−0.328 −0.308[d]	163	−0.246	0.041
3	600(112), 263 (15380), 289 (6580)	2.29	2.02	160	141	143	0.780	1.089	0.783	0.850	0.544	−0.238 -	−0.396–0.386[d]	158	−0.317	0.112

[a] Concentration: 1×10^{-3} M in aqueous solution at 25 °C.
[b] Measured at 70 K in methanol:DMF solution (8:2); $A_{||}$ and $A_{\perp}$ in 10^{-4} cm^{-1}. $\alpha^2 = A_{||}/0.036 + (g_{||} - 2.0023) + 3/7\ (g_{\perp} - 2.0023) + 0.04$. $K_{||} = \alpha^2\beta^2$ and $K_{\perp} = \alpha^2\gamma^2$, $K^2_{||} = (g_{||} - 2.0023)\ \Delta E\ (d_{xy} - d^2_{x-y})/8\lambda_0)$, $K^2_{\perp} = (g_{\perp} - 2.0023)\ \Delta E\ (d_{xz,yz} - d^2_{x-y})/2\lambda_0)$.
[c] Concentration:1×10^{-3} M in aqueous solution 25 °C (reference: Ag/Ag^+; supporting electrolyte: 0.1 M NaCl; scan rate = 50 mV s^{-1}). To convert to $E_{1/2}$ versus NHE, add + 0.205 V.
[d] in acetonitrile.

(Table 2). In general, α^2 values would be close to unity for ionic bonding and it decreases with increasing covalency [40]. The orbital reduction factors $K_{||} = \alpha^2\beta^2$ and $K_{\perp} = \alpha^2\gamma^2$ were calculated and are in the range of 0.764–0.934 and 0.408–0.859 respectively. All the complexes exhibit $K_{||} > K_{\perp}$, reveals the persistence of significant amount of out-plane π-bonding in all complexes, whereas $K_{||} = K_{\perp}$ for pure σ-bonding and $K_{||} < K_{\perp}$ in-plane π-bonding are reported [44].

2.3. Redox properties

The redox properties of **1**–**3** have been studied by cyclic voltammetry (CV) using a three-electrode cell configuration in water. A platinum sphere/glassy carbon, a platinum wire, and Ag/Ag^+ were used as working, auxiliary and reference electrodes respectively. Sodium chloride was used as supporting electrolyte. The complexes **1 – 3** exhibited Cu(II)/Cu(I) redox couples, which are highly deviated from reversibility. The ΔE (145–163 mV) values correspond to quasi-reversible process [44]. The aqueous solution of **1** exhibit Cu(II)/Cu(I) redox potentials at −0.213 V with cathodic (Ep_c) and anodic (E_{pa}) peaks around −0.285 and −0.140 V respectively (Fig. 3, Table 2). On introducing an additional methylene spacer connecting pyridyl arm and 1,4-diazepane backbone in **1** to obtain **2**, exhibited a slightly negative shift in Cu(II)/Cu(I) redox potential (−0.246 V). It is shifted to a more negative potential for **3** (−0.317 V) due to electron-releasing substituents at pyridyl arm. In acetonitrile, the complexes exhibit only cathodic peaks Ep_c (−0.269 to −0.386 V) and their corresponding anodic peaks are ill-defined (Fig. S4). The Cu(II)/Cu(I) redox potential values of **1**–**3** are higher than those of reported analogs CuN4 complexes ($E_{1/2}$, −0.349 to −0.404 V) [24]. This illustrates that the higher Lewis acidity of present CuN3 complexes and hence expected to show higher rates of the oxidative cleavage reaction (cf. below). The measured redox potentials were converted into NHE (normal hydrogen electrode) by adding +0.205 V to compare those of LPMOs and other reported models. The Cu(II)/Cu(I) redox potentials of **1**–**3** (0.008–0.112 V vs. NHE) is slightly higher than those of previously reported model complexes (0.005–0.05 V vs. NHE) [13]. However, these redox potentials are lower than those of LPMO enzyme (0.15 V to 0.37 V vs NHE) [3–5,30].

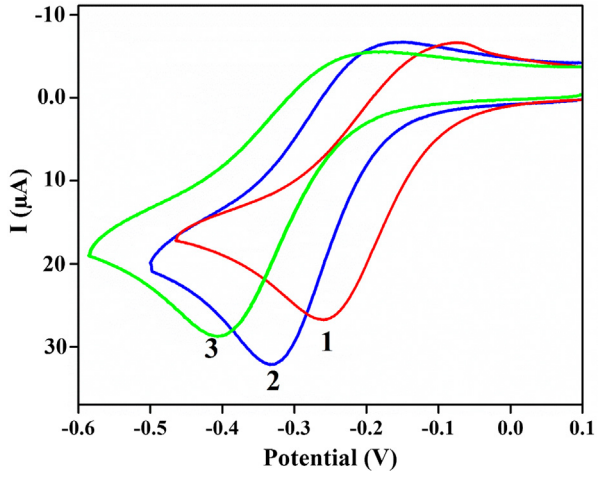

Fig. 3. Cyclic voltammograms of complexes **1** – **3** (1×10^{-3} M) in water at 25 °C. Supporting electrolyte: 0.1 M NaCl. Working electrode: Glassy carbon, Reference electrode: Ag/Ag^+ and counter electrode: Pt wire. Scan rate: 100 mV.

2.4. Oxidative cleavage of *p*-nitrophenyl-β-D-glucopyranoside

The *p*-nitrophenyl-β-D-glucopyranoside was used as a model substrate for studying LPMO reactivity and aqueous hydrogen peroxide (30%) was employed as an oxygen source in the presence of one equivalent of Et_3N. The kinetics of LPMO-like oxidative cleavage reaction was monitored in water by following the formation of the absorption band at 400 nm corresponding to the *p*-nitrophenol (Fig. 4). The rate constant (k_{obs}) for *p*-nitrophenol formation was calculated as 3.19×10^{-3} s^{-1} for **1**, which is almost identical to that of **2** (3.96×10^{-3} s^{-1}). But they are lower than the rate of formation observed for **3** (5.26×10^{-3} s^{-1}) (Figs. 4, S6 and S7 and Table 3), which is due to the reaction rate accelerated by more steric crowding and electron releasing groups [17,38,45]. The electron releasing groups in pyridyl arm of **3** possibly mobilize more electron density on copper center for the facile formation of Cu^{II}-OOH intermediate as compared to **1** and **2** (cf. below). The steric hindrance offered by 1,4-diazepane backbone likely facilitate faster product release. The rate of oxidative cleavage reaction follows the order of **3** > **2** > **1** >. The formation of *p*-nitrophenol was analyzed and quantified by GC/GC-MS (Figs. S8 and S9).

In separate experiments, the reaction of *p*-nitrophenyl-β-D-glucopyranoside (200 μM) with aqueous hydrogen peroxide (200 μM) in the presence of complexes (2.5 μM, 1.25 mol%) and

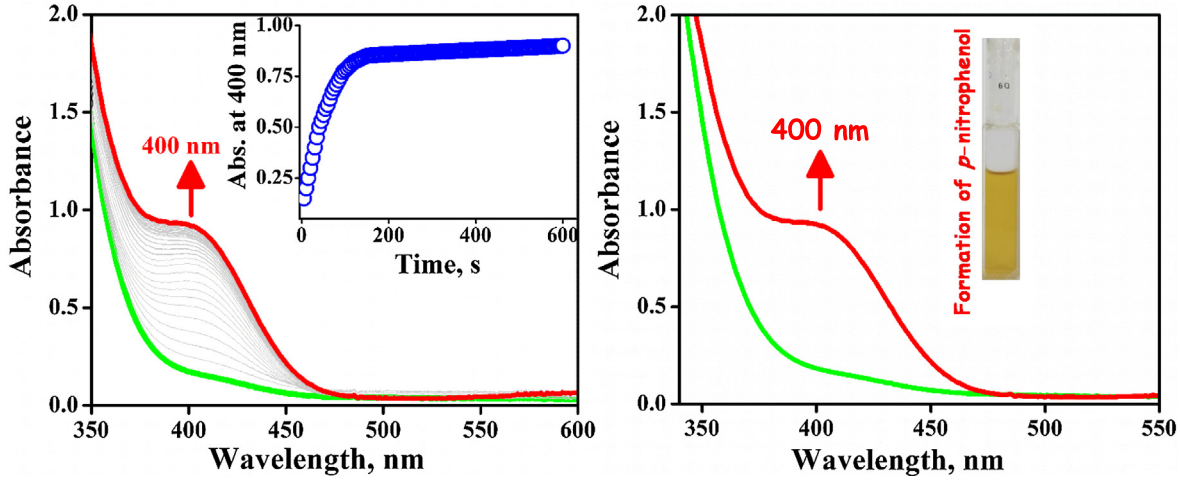

Fig. 4. (a) The electronic spectral changes for the reaction of **3** (1×10^{-4} M) with the substrate (1×10^{-4} M), H_2O_2 (10 equivalent) and Et_3N (1 equivalent) in aqueous solution at 25 °C. (b) Comparison of the spectral changes before and after the formation of *p*-nitrophenol.

Table 3
Oxidative cleavage of *p*-nitrophenyl-*β*-D-glucopyranoside by complexes **1** – **3** using H_2O_2 and Et_3N.

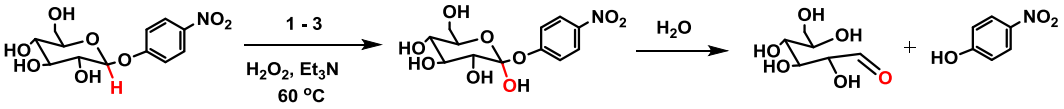

Complex	k_{obs} ($\times 10^{-3}$ s^{-1})[a]	$t_{1/2}$ (s)[d]	[H_2O_2] mmol	Yield[e] (%)	TON	TOF (h^{-1})
1	3.19 ± 0.1[b]	217	0.1	28.4	118	59
	1.61 ± 0.2[c]		0.5	69.4	289	144
2	3.96 ± 0.2[b]	175	0.1	31.6	126	63
	3.32 ± 0.1[c]		0.5	72.4	290	145
3	5.26 ± 0.2[b]	132	0.1	38.3	147	73
	9.06 ± 0.1[c]		0.5	78.4	300	150

[a] k_{obs} = 1 + log(Abs) vs time.
[b] Formation of *p*-nitrophenol in H_2O.
[c] Formation of Cu^{II}-OOH species in H_2O.
[d] $t_{1/2} = 0.693/k_{obs}$.
[e] Isolated Yields.

triethylamine (2.5 μM) was carried out for 2 h at 60 °C. They afforded *p*-nitrophenol and D-allose as products (Figs. S9 and S10, Table 3), but we have calculated the yield of *p*-nitrophenol in order to obtain a direct correlation with kinetic parameters. The catalyst **3** showed highest yield of *p*-nitrophenol (64.8%; TON, 249) than **2** (59.3%; TON, 237) and **1** (48.5%; TON, 202). The catalytic efficiency of complexes followed the order of **3 > 2 > 1**, which is similar to the trend obtained by kinetics. The rate of the oxidative cleavage reaction is seemingly influenced by the Cu(II)/Cu(I) redox potentials. Indeed, the highest rate of *p*-nitrophenol conversion was exhibited by **3**, which has lower Cu(II)/Cu(I) redox potential (−0.317 V vs Ag/Ag^+) than **1** and **2**. Additionally, the oxidative cleavage reaction was performed at 30 °C using most active catalyst **3** under the identical condition, which afforded 45.2% yield of p-nitrophenol with TON, 174. The highest yield of *p*-nitrophenol formation is interesting, which is the best catalytic efficiency achieved for LPMO like oxidative cleavage reactions. It is concomitantly higher than that of previously reported model complexes by Simaan and co-workers, where TON of 50 is reported at longer reaction time (24 h) [13]. In the present work, increases in the reaction time for more than 2 h showed a slight enhancement in *p*-nitrophenol formation for all complexes (Fig. 5a and Table S1). The reactions performed in the absence of catalyst or H_2O_2 or Et_3N showed only a trace amount of *p*-nitrophenol under an identical condition at 60 °C. This indicates the involvement of the oxidative cleavage reaction rather than simple hydrolysis (Figs. S11 and S12). Further, a trace amount of *p*-nitrophenol was observed while using $CuSO_4$ as the catalyst. The catalytic reactions were performed for various concentration of H_2O_2 (0.1–0.5 mmol) (Figs. 5b and S13, Table S2). The higher yield of *p*-nitrophenol was achieved only while using 0.5 mmol of H_2O_2 without increasing the catalyst loading. As expected, the catalyst **3** showed the highest yield (78.4%; TON, 300) than **1** (69.4%; TON, 289) and **2** (72.4%; TON, 290). On the other hand, a decrease in the yield was noted while lowering the amount of H_2O_2 used (0.1 mmol), which exhibited, 28.4%, 31.6% and 38.3% for **1 – 3** respectively. Thus, the efficiency of oxidative cleavage reactions and yield of *p*-nitrophenol depends on the amount of H_2O_2 used. The catalytic efficiency is also depending on the catalyst loading, use of 6.25 mol% catalyst showed a maximum yield up to 76.8% (Fig. 5c and Table S3) but with lower TON. In addition, the catalytic reactions were performed over various temperatures (25–100 °C) under the identical condition, showed the product yield was enhanced linearly while increasing temperature (Fig. S14, Table S4) and maximum yield up to 70.6% was noticed for **3** at 100 °C. Further, to verify the selectivity of the oxidative cleavage reaction, the catalysis was performed for primary and secondary alcohol such as benzyl alcohol and 1-phenylethanol as substrates using most active catalyst **3** (2.5 μM) and H_2O_2 (200 μM) at 60 °C. It showed no oxidized products and only the substrates were recovered quantitatively (Figs. S15 and S16).

The regioselective oxidative cleavage reaction is possibly operating via Cu^{II}-OOH key intermediate, which was characterized by electronic spectral studies (Figs. 6, S17–S19) and its structure was optimized by DFT calculations. Addition of 10 equivalents of 30% H_2O_2 and one equivalent Et_3N to **1 – 3** exhibited O (π^*_σ) → Cu LMCT transition around 375 nm corresponds to Cu^{II}-OOH species in water [46]. Thereat, base Et_3N seemingly facilitates the binding of H_2O_2 with copper(II) center to form Cu^{II}-OOH species. The rate of formation was calculated by monitoring the growth of this LMCT transition, which are calculated as **1** (1.61×10^{-3} s^{-1}), **2** (3.32×10^{-3} s^{-1}) and **3** (9.06×10^{-3} s^{-1}) (Fig. S19 and Table 3). The highest rate of formation was noticed for **3,** which is coextensive with the faster rate of formation of *p*-nitrophenol and higher yield. The intermediate also exhibited d-d transition around 635 (ε, 24 M^{-1} cm^{-1}), 630 (ε, 27 M^{-1} cm^{-1}) and 630 nm (ε, 31 M^{-1} cm^{-1}) for **1–3** respectively, which indicates the persistence of the copper(II) oxidation state (Fig. S20). This is further confirmed by electrochemical studies, where no concomitant changes in the redox potential were observed for **1** in the presence of H_2O_2 and Et_3N over 15 min at room temperature (Fig. S21). Further, the addition of 10 equivalents of *tert*-butylperoxide and Et_3N (1 equivalent) to **3** showed a formation of LMCT band at 380 nm (ε, 182 M^{-1} cm^{-1}) corresponds to the formation of copper-bound *tert*-butylperoxo species (Fig. S22) [47]. It was further confirmed by solution FT-IR spectra (Fig. 7), where Cu—O and O—O stretching frequencies appeared at 750 and 925 cm^{-1} [48]. On the other hand, it was also suggested that high-valent copper oxo-species or radicals derived from hydroperoxo species could be possible intermediates for regioselective oxidative cleavage of polysaccharides [16]. The catalysis was performed in the presence of radical trapping agent TEMPO (2,2,6,6-tetramethylpiperidin-1-yl-oxyl) using the most efficient catalyst **3** under an identical condition at 60 °C. It showed no perceptible change in the product yield and 64.5% of yield was noticed, which clearly eliminates the possibility of radical based reaction pathways under our experimental condition [49]. On the other hand, use of dimethylpyrroline N-oxide (DMPO) as a radical trapping agent

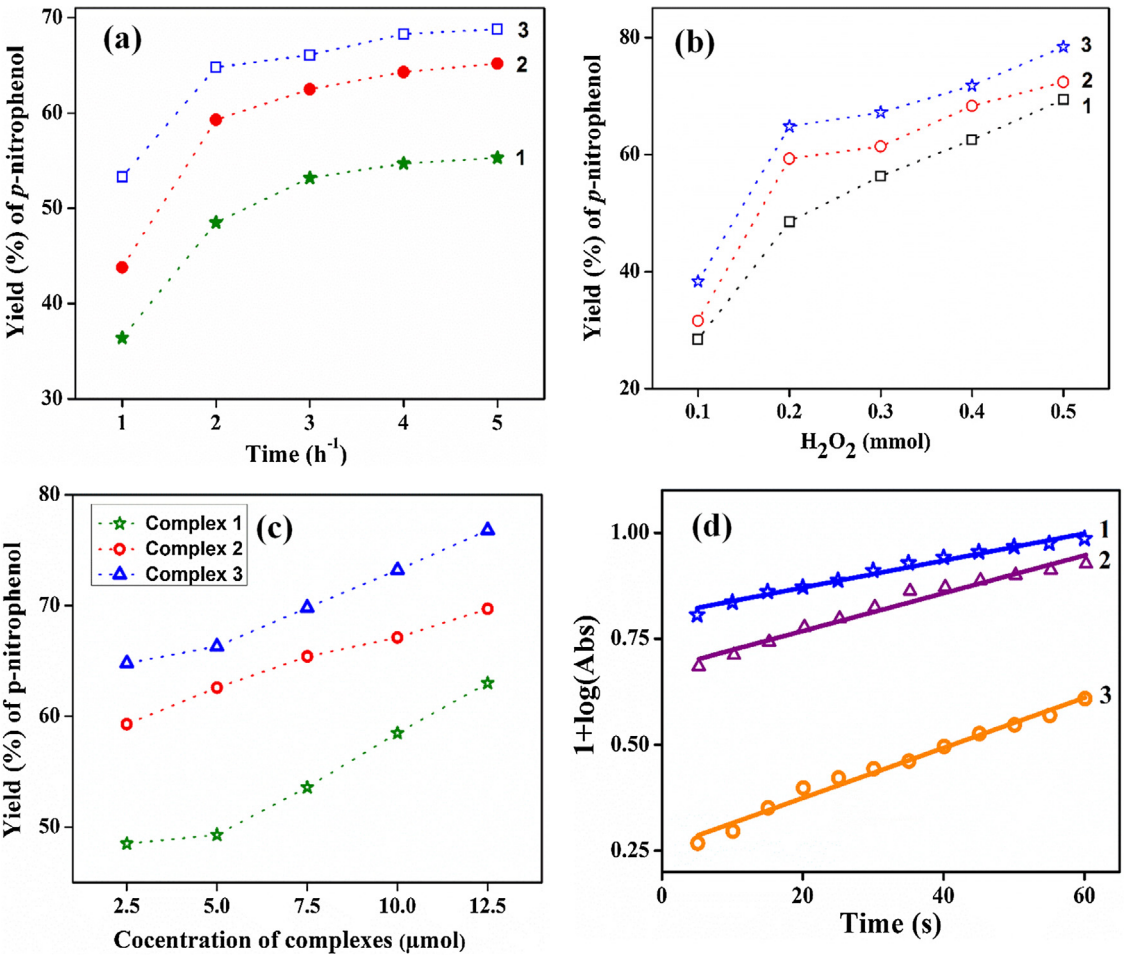

Fig. 5. (a) Time-dependent formation of the *p*-nitrophenol for **1**–**3** with substrate (200 μM), Et_3N (2.5 μM) and $[H_2O_2]$ = 200 μM (b) H_2O_2 dependent formation of the *p*-nitrophenol. (c) The plot of yield versus various concentration of complexes (d) The calculation of k_{obs} for the formation of *p*-nitrophenol for **1 – 3** by the plot of [1 + log(Abs)] vs time.

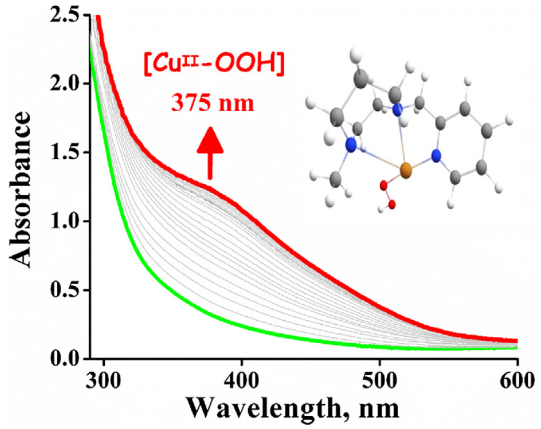

Fig. 6. The electronic spectral change for **1** (5×10^{-5} M) reaction with H_2O_2 (10 equivalent) in the presence of Et_3N (1 equivalent) in aqueous solution. Inset: Optimized structure of [(L1)Cu^{II}-OOH].

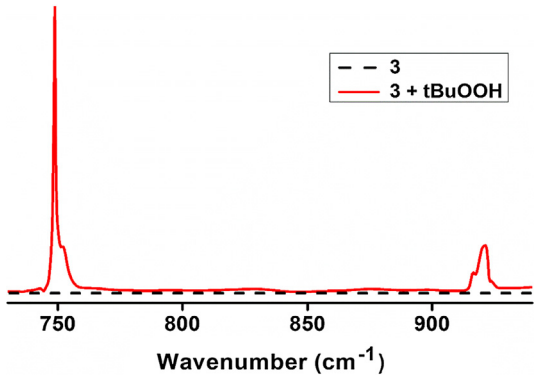

Fig. 7. Solution-state FT-IR spectra for **3** (5×10^{-5} M) reaction with ^{t}BuOOH (10 equivalent) in the presence of Et_3N (1 equivalent) upon the formation of [Cu^{II}-OO^{t}Bu] intermediate.

was not helpful, where almost identical quantities of DMPO-OH radical were detected by EPR in the presence or absence of a catalyst.

The key Cu^{II}-OOH intermediate may be generated by the reaction of hydrogen peroxide without altering the copper coordination geometry and oxidation state [14]. Very similar Cu^{II}-OOH species was reported by Simaan and co-workers. In literature, several Cu-OOH intermediates are reported in the presence of an organic solvent at low temperature using different copper complexes [14]. But only a few of complexes were reported to stabilize the Cu^{II}-OOH intermediate in aqueous solution [50]. The electron density of the copper center apparently affects the formation of Cu^{II}-OOH intermediate and catalysis. Density functional theory (DFT) calculations were performed for **1** as the representative

example using the B3LYP 6-31G (d) (for C, H, N, O, and Cl) and the LANL2DZ (for Cu) basis sets in the Gaussian 09 program [51]. The calculations were carried out in water solvent using Conductor-like Polarizable Continuum Model (C-PCM). All possible intermediate species of **1** were optimized, the computed bond parameters and relative energies of different species are given in the supporting information (Figs. S23–S26). The absorption spectra of Cu-OOH species of **1** was calculated by TD-DFT method, showed O → Cu^{II} LMCT transition at 383 nm and is comparable with the experimentally observed value at 375 nm. TD-DFT studies showed that the singly occupied molecular orbital (SOMO) of **1** localized mainly on copper centre along with oxygen and nitrogen atoms, whereas the lowest unoccupied molecular orbital (LUMO) localized on pyridyl moiety of the ligand. The overall reaction is seemingly exothermic ($\Delta E = -26.7$ kcal/mol). Thus, the spectral data and DFT calculations indicate that Cu^{II}-OOH species (intermediate **D**) may be the key intermediate for oxidative cleavage of the C—O bond. In fact, our model complexes have almost similar ligating donors and backbone as in 'histidine brace' of LPMOs but with a slight variation on the structural motif. The correlation between the formation/decay of the intermediates and the production of p-nitrophenolate became difficult as due to the electronic spectral overlap of substrate and intermediate.

3. Conclusions and relevance to LPMOs

A relevant structurally well-defined copper(II) complexes of 3 N ligands based on diazepane backbone have been synthesized as models for LPMOs and are characterized by spectral methods. The molecular structure of the complexes adopts very similar distorted square-pyramidal coordination geometry with the CuN_3O_2 core as in the LPMOs enzyme. The position of d-d transitions and EPR parameters support the existence of square-based geometry of complexes in solution, which are almost identical to LPMOs. More interestingly, the formation of [Cu^{II}-OOH] intermediate characterized by spectral methods and DFT calculation. The *p*-nitrophenyl-*β*-D-glucopyranoside and hydrogen peroxide were used as a model substrate and oxygen source respectively. The present model complexes showed a much higher yield of *p*-nitrophenol up to 78.4% (TON, 300) via regioselective oxidative cleavage pathway in water. The formation of product and kinetic information were obtained by its characteristic electronic spectral signature at 400 nm. The redox potentials of complexes seemingly influenced by the electronic nature of the ligands, which affects oxidative cleavage reaction. Thus, the electron density of the copper(II) center affects the catalytic efficiency directly as evidence that the complex with higher electron density on copper facilitates the formation of Cu^{II}-OOH species and C-O cleavage product.

4. Experimental

4.1. Materials

1-Methylhomopiperazine, 2-picolylchloride hydrochloride, 2-vinylpyridine, 2-chloromethyl-4-methoxy-3,5-dimethylpyridine hydrochloride, copper(II)perchlorate hexahydrate, chloroform-D, triethylamine, 2,2,6,6-tetramethylpiperidin-1-yl-oxyl (TEMPO), dimethylpyrroline N-oxide (DMPO), benzyl alcohol and 1-phenylethanol were purchased from Sigma-Aldrich· H_2O_2 and *p*-nitrophenyl-*β*-D-glucopyranoside were purchased from TCI chemicals. Sodium bicarbonate, magnesium sulfate was purchased from SRL chemicals. Sodium hydroxide, acetic acid, silica gel were purchased from Merck Chemicals.

4.2. Physical measurement

All reactions were carried out under an atmosphere of dry nitrogen. Glassware was oven dried prior to use. All the solvents were used after appropriate distillation or purification. NMR spectra were recorded on 300 MHz Bruker instrument. Chemicals shifts values and coupling constants are given in ppm and Hz respectively. Electron Paramagnetic Resonance (EPR) measurements were recorded using Bruker EMX Plus EPR Spectrometer. ESI-Mass spectra were recorded using a Thermo LC-MS instrument. UV–vis spectra and kinetic data were obtained on Agilent diode array spectrometer (Agilent 8453). FT-IR measurements were recorded using Thermo Nicolet 6700. Elemental analyses were carried out using a Heraeus Vario Elemental automatic analyzer. Cyclic Voltammetry (CV) experiments were performed using a three-electrode cell configuration. A platinum sphere (acetonitrile medium) and glassy carbon (aqueous), platinum wire and Ag(s)/Ag^+ were used as working, auxiliary and reference electrodes respectively. The Bu_4NClO_4 and NaCl were used as supporting electrolytes in acetonitrile and water respectively. The $E_{1/2}$ values were observed under identical conditions for various scan rates. GC-MS and GC analysis performed on Agilent 5977E GCMSD using HP-5 MS ultra-inert (30 m × 250 μm × 0.25 μm) capillary column.

4.3. Single crystal X-ray structure analysis

The experiment was performed on Agilent Technologies Supernova-E CCD diffractometer. The suitable single crystals of **1** and **2** suitable size were selected from the mother liquor and immersed in paraffin oil, then mounted on the tip of a glass fiber. The structures were solved by direct methods using the program SHELXS-2013. Refinement and all further calculations were carried out using SHELXL-2013. The H-atoms were included in calculated positions and treated as riding atoms using the SHELXL default parameters. The non-H atoms were refined anisotropically, using weighted full-matrix least-square on F^2. CCDC 1,554,182 and CCDC 1,554,184 are containing the supplementary crystallographic data for this paper. This data can be obtained free of charge from The Cambridge Crystallographic Data Centre via ww.ccdc.cam.ac.uk/data request/cif.

4.4. DFT methods

All theoretical calculations were performed with the Gaussian 09 program package [51]. The geometry optimizations were performed by using density functional theory (DFT) methods with the Becke3–Lee–Yang–Parr hybrid functional (B3LYP). The basis set 6-31G (d) is applied for C, H, N, O and Cl, and the LANL2DZ applied for Cu atom. Solvent effects were accounted in accordance with the experimental conditions and water used as a solvent by utilizing Conductor-like Polarizable Continuum Model (C-PCM). Electronic transition energies for all models were calculated using time-dependent DFT (TDDFT). The total energies of each complex were obtained from frequency calculations. Visualization of optimized geometry of the complexes and molecular orbitals were rendered by using Chemcraft software [52].

4.5. Synthesis of ligands

4.5.1. Synthesis of 4-methyl-1-[(pyridin-2-yl-methyl)]-1,4-diazepane (L1)

The NaOH (0.795 g, 20 mmol) in 10 mL was added dropwise to an aqueous solution of 2-picolylchloride hydrochloride (1.64 g, 10 mmol) in another 10 mL at 0 °C. 1-methyl homopiperazine (1.14 g, 10 mmol) in 20 mL of water was then added to this mixture over 15 min. The mixture was stirred in a loosely sealed flask

at room temperature for three days. The reaction mixture was then extracted with $CHCl_3$ (3 × 50 mL). The organic layer was washed with saturated sodium hydrogen carbonate solution, evaporated, and then dried (Na_2SO_4). The organic solvent was removed on a rotary evaporator to yield the crude product as a pale-yellow oil. The pure product was obtained by extracting the oil once again with ethyl acetate. Yield, 1.287 g (62.4%). ^{1}H NMR (300 MHz, $CDCl_3$), δ, 8.4 (d, 1H, *J* = 4.03 Hz), 7.5 (t, 1H, *J* = 7.66 Hz), 7.3 (d,1H, *J* = 7.78 Hz), 7.0 (t, 1H, *J* = 7.55 Hz), 3.7 (s, 2H), 2.7–2.6 (m, 4H), 2.6–2.5 (m, 4H), 2.2 (s, 3H), 1.7 (pentet, 2H, *J* = 11.77 Hz). ^{13}C NMR ($CDCl_3$), δ, 46.15 (CH_3), 26.51, 53.62, 54.34, 56.21, 57.40, 64.75, (CH_2), 121.80, 122.85, 136.27, 146.87, 159.32 ppm (ArC). ESI-MS (*m*/*z*): $[M + H]^+$, 206.23.

4.5.2. Synthesis of 4-methyl-1-[(2-(pyridine-2-yl)ethyl]-1,4-diazepane (L2)

To a solution of 1-methylhomopiperazine (5.8 mmol, 0.662 g) in methanol (30 mL), acetic acid (7.2 mmol, 0.432 g) and 2-vinylpyridine (14.4 mmol, 1.514 g) were added. The reaction mixture was then warmed to 65 °C and stirred for two days. The mixture was cooled to room temperature, and the volatiles was removed under reduced pressure. The remaining red-brown oil was dissolved in H_2O and carefully made basic using solid NaOH. It was subsequently extracted three times with toluene. The removal of toluene from the combined organic phases left the crude product as a red oil, which was purified by repeated extraction with small amounts of hexane. The solvent was removed under vacuum to give light yellow oil; yield, 0.62 g (40%).^{1}H NMR (300 MHz, $CDCl_3$), δ, 8.4 (d, 1H, *J* = 4.16 Hz), 7.5 (t, 1H, *J* = 7.71 Hz), 7.4 (d, 1H, *J* = 7.76 Hz), 7.0 (t, 1H, *J* = 7.65 Hz), 2.9 (d, 4H, *J* = 1.97 Hz), 2.8 (m, 2H), 2.73 (m, 2H), 2.73 (m, 4H), 2.6 (s, 3H), 1.8 (pentet, 2H, *J* = 11.79 Hz). ^{13}C NMR ($CDCl_3$), 46.51 (CH_3), 26.70, 35.89, 46.51, 49.83, 55.66, 53.81, 56.57, 57.40, 58.25, (CH_2), 121.00, 123.12, 136.27, 146.88, 160.17 ppm (Ar). ESI-MS (*m*/*z*): $[M + H]^+$, 220.18.

4.5.3. Synthesis of 1-(4-methoxy-3,5-dimethylpyridin-2-yl)methyl)-4-methyl-1,4-diazepane (L3)

A slightly modified procedure of the previously reported method was used to synthesize ligand. Aqueous solution (10 mL) of NaOH (0.795 g, 20 mmol) was added dropwise to an aqueous solution (10 mL) of 2-chloromethyl-4-methoxy-3,5-dimethylpyri dine hydrochloride (2.22 g, 10 mmol) at 0 °C. Further addition of 1-methylhomopiperaine (1.142 g, 10 mmol) in 20 mL of water was then added to this mixture over 15 min. The mixture was stirred in a loosely sealed flask at room temperature for three days. The reaction mixture was then extracted with $CHCl_3$ (3 × 50 mL). The organic layer was washed with saturated sodium hydrogen carbonate solution, evaporated, and then dried (Na_2SO_4). The organic solvent was removed on a rotary evaporator to yield the crude product as a pale-yellow oil. The pure product was obtained by extracting the oil once again with ethyl acetate. Yield, 1.6 g (60%). ^{1}H NMR (300 MHz, $CDCl_3$), ^{1}H NMR (300 MHz, $CDCl_3$), δ, 8.20 ppm (s, 1H), 3.7 (s, 3H), 3.56 (s, 2H), 2.7–2.68 (m, 8H), 2.3 (s, 6H), 2.18 (s, 3H), 1.79 (pentet, 2H). ^{13}C NMR ($CDCl_3$), 164.44, 157.65, 148.56, 126.59, 125.37, 63.01, 60.21, 58.37, 56.97, 54.66, 53.88, 47.07, 27.48, 13.6, 11.3 ppm.

4.6. Synthesis of copper(II) complexes

Caution! During handling of the perchlorate salts of metal complexes with organic ligands, care should be taken because of the possibility of explosion.

[Cu(L1)(H_2O)ClO_4]ClO_4 ***(1)***: To the solution of ligand (0.205 g, 1 mmol) in MeOH (8 mL) and $Cu(ClO_4)_2{\cdot}6H_2O$ (0.37 g, 1 mmol) in H_2O (2 mL) was added dropwise under stirring at room temperature for 3 h. The color changed to a dark blue color. Solvent removal under reduced pressure gave a blue colored residue which was washed twice (10 mL each) with hexane to remove the excess ligand. The compound was then dried under high vacuum over fused $CaCl_2$. Recrystallization from MeOH gave a blue colored crystal suitable for X-ray crystallography analysis. Yield, 0.28 g (96%). ESI-MS, $[C_{12}H_{19}CuN_3O_4Cl]^+$, *m*/*z*, 368.14. Analytically calculated elements for $C_{12}H_{21}CuN_3O_9Cl_2$: C, 29.67; H, 4.36; N, 8.65%. Found: C, 29.65; H, 4.37; N, 8.64%.

[Cu(L2)(H_2O)ClO_4]ClO_4 ***(2)***: The above procedure has been followed to synthesize **2** using ligand L2 instead of L1 in MeOH: H_2O (8:2) solution. The blue colored solid was isolated with a yield of 0.312 g (72.4%). Slow evaporation of the mother liquor at room temperature afforded single crystals suitable for X-ray analysis. ESI-MS, $[C_{13}H_{23}CuN_3O_5Cl]^+$, *m*/*z*, 399.20. Analytically calculated elements for $C_{13}H_{23}CuN_3O_9Cl_2$: C, 31.24; H, 4.64; N, 8.41%. Found: C, 31.23; H, 4.63; N, 8.39%.

[Cu(L3)(H_2O)ClO_4]ClO_4 ***(3)***: This complex was also prepared by the similar reaction of $Cu(ClO_4)_2{\cdot}6H_2O$ with ligand L3 in MeOH: H_2O (8:2) solution. Yield, 0.28 g (86%). ESI-MS, $[C_{15}H_{27}CuN_3O_5Cl]^+$, *m*/*z*, 427.25. Analytically calculated elements for $C_{15}H_{27}CuN_3O_{10}Cl_2$: C, 33.13; H, 5.00; N, 7.73%. Found: C, 33.11; H, 4.98; N, 7.71%.

4.7. Oxidation of p-nitrophenyl-β-D-glucopyranoside

The catalytic activity of the copper(II) complexes **1**–**3** was assessed using the oxidation of *p*-nitrophenyl-β-D-glucopyranoside by H_2O_2 in water at the mild condition. Reaction condition, the model substrate (200 μmol), a catalytic amount of the complex (2.5 μmol, 1.25 mol %), aqueous hydrogen peroxide (200 μmol), triethylamine (2.5 μmol) was dissolved in H_2O (3.0 mL). The mixture was stirred at 60 °C for 2 h, then the reaction was quenched at the appropriate time by passing on silica column. Conversion of *p*-nitrophenol formation was analyzed and quantified by GC/GC-MS. The blank reaction performed using identical condition but in the absence of catalyst or H_2O_2.

4.8. Kinetic studies

Kinetic experiments of the *p*-nitrophenol formation were studied by spectrophotometrically as time-dependent measurement at 25 °C. A solution of the stoichiometric amount of complexes **1**–**3** (1×10^{-4} M) was treated with *p*-nitrophenyl-β-D-glucopyranoside (1×10^{-4} M), aqueous H_2O_2 (10 equivalent) and pre-treated with one equivalent of Et_3N in H_2O at 25 °C.

Acknowledgments

We acknowledge Science and Engineering Research Board (SERB), New Delhi and Board of Research in Nuclear Science (BRNS), Mumbai for funding.

Appendix A. Supplementary material

Supplementary data to this article can be found online at https://doi.org/10.1016/j.jcat.2019.03.019.

References

[1] M.E. Himmel, S.Y. Ding, D.K. Johnson, W.S. Adney, M.R. Nimlos, J.W. Brady, T.D. Foust, Science 315 (2007) 804–807.
[2] R.A. Sheldon, Green Chem. 16 (2014) 950–963.
[3] G.R. Hemsworth, E.M. Johnston, G.J. Davies, P.H. Walton, Trends Biotechnol. 33 (2015) 747–761.
[4] V.V. Vu, S.T. Ngo, Coord. Chem. Rev. 368 (2018) 134–157.
[5] W.T. Beeson, V.V. Vu, E.A. Span, C.M. Phillips, M.A. Marletta, Annu. Rev. Biochem. 84 (2015) 923–946.
[6] S.T. Merino, J. Cherry, Adv. Biochem. Eng. Biotechnol. 108 (2007) 95–120.

[7] P.V. Harris, D. Welner, K.C. McFarland, E. Re, J.C. Navarro Poulsen, K. Brown, R. Salbo, H. Ding, E. Vlasenko, S. Merino, F. Xu, J. Cherry, S. Larsen, L. Lo Leggio, Biochemistry 49 (2010) 3305–3316.
[8] G. Vaaje-Kolstad, B. Westereng, S.J. Horn, Z. Liu, H. Zhai, M. Sorlie, V.G. Eijsink, Science 330 (2010) 219–222.
[9] S.J. Horn, G. Vaaje-Kolstad, B. Westereng, V.G.H. Eijsink, Biotechnol. Biofuel. 5 (2012) 45–56.
[10] M.D. Sweeney, F. Xu, Catalysts 2 (2012) 244–263.
[11] M. Dimarogona, E. Topakas, P. Christakopoulos, Appl. Microbiol. Biotechnol. 97 (2013) 8455–8465.
[12] I. Castillo, A.C. Neira, E. Nordlander, E. Zeglio, Inorg. Chim. Acta 422 (2014) 152–157.
[13] A.L. Concia, M.R. Beccia, M. Orio, F.T. Ferre, M. Scarpellini, F. Biaso, B. Guigliarelli, M. Reglier, A.J. Simaan, Inorg. Chem. 56 (2017) 1023–1026.
[14] (a) A. Wada, M. Harata, K. Hasegawa, K. Jitsukawa, H. Masuda, M. Mukai, T. Kitagawa, H. Einaga, Angew. Chem. Int. Ed. 37 (1998) 798–800;
(b) M. Kodera, T. Kita, I. Miura, N. Nakayama, T. Kawata, K. Kano, S. Hirota, J. Am. Chem. Soc. 123 (2001) 7715–7716;
(c) T. Osako, S. Nagatomo, Y. Tachi, T. Kitagawa, S. Itoh, Angew. Chem. Int. Ed. 41 (2002) 4325–4328;
(d) T. Fujii, A. Naito, S. Yamaguchi, A. Wada, Y. Funahashi, K. Jitsukawa, S. Nagatomo, T. Kitagawa, H. Masuda, Chem. Commun. (2003) 2700–2701;
(e) E.A. Span, M.A. Marletta, Curr. Opin. Struct. Biol. 35 (2015) 93–99;
(f) P.H. Walton, G.J. Davies, Curr. Opin. Chem. Biol. 31 (2016) 195–207;
(g) T. Tsuji, A.A. Zaoputra, Y. Hitomi, K. Mieda, T. Ogura, Y. Shiota, K. Yoshizawa, H. Sato, M. Kodera, Angew. Chem. Int. Ed. 56 (2017) 7779–7782.
[15] (a) S. Itoh, Acc. Chem. Res. 48 (2015) 2066–2074;
(b) A. Kunishita, M. Kubo, H. Sugimoto, T. Ogura, K. Sato, T. Takui, S. Itoh, J. Am. Chem. Soc. 131 (2009) 2788–2789.
[16] (a) N. Gagnon, W.B. Tolman, Acc. Chem. Res. 48 (2015) 2126–2131;
(b) D. Dhar, G.M. Yee, T.F. Markle, J.M. Mayer, W.B. Tolman, Chem. Sci. 8 (2017) 1075–1085.
[17] T. Dhanalakshmi, E. Suresh, H. Stoeckli-Evans, M. Palaniandavar, Eur. J. Inorg. Chem. (2006) 4687–4695.
[18] R.A. Geiger, S. Chattopadhyay, V.W. Day, T.A. Jackson, J. Am. Chem. Soc. 132 (2010) 2821–2831.
[19] R. Mayilmurugan, H. Stoeckli-Evans, M. Palaniandavar, Inorg. Chem. 47 (2008) 6645–6658.
[20] J.A. Halfen, J.M. Uhan, D.C. Fox, M.P. Mehn, L. Que, Inorg. Chem. 39 (2000) 4913–4920.
[21] M. Schmidt, D. Wiedemann, B. Moubaraki, N.F. Chilton, K.S. Murray, K.R. Vignesh, G. Rajaraman, A. Grohmann, Eur. J. Inorg. Chem. (2013) 958–967.
[22] K. Visvaganesan, E. Suresh, M. Palaniandavar, Dalton Trans. (2009) 3814–3823.
[23] A.W. Addison, T.N. Rao, J. Reedijk, J. van Rijn, G.C. Verschoor, J. Chem. Soc., Dalton Trans. 7 (1984) 1349–1356.
[24] S. Muthuramalingam, S. Subramaniyan, T. Khamrang, M. Velusamy, R. Mayilmurugan, Chem. Select 2 (2017) 940–948.
[25] A.R. Amundsen, J. Whelan, B. Bonich, J. Am. Chem. Soc. 99 (1977) 6730.
[26] M.J. Ettinger, Biochemistry 13 (1974) 1242–1247.
[27] R. Uma, R. Viswanathan, M. Palaniandavar, M. Lakshminarayanan, J. Chem. Soc., Dalton Trans. 8 (1994) 1219–1226.
[28] J.P. Klinman Chem. Rev. 96 1996 2541 2561
[29] D. Cai, J.P. Klinman, Biochemistry 33 (1994) 7647–7653.
[30] S. Garajova, Y. Mathieu, M.R. Beccia, C. Bennati-Granier, F. Biaso, M. Fanuel, D. Ropartz, B. Guigliarelli, E. Record, H. Rogniaux, B. Henrissat, J.G. Berrin, Sci. Rep. 6 (2016) 28276.
[31] N.J. Ray, L. Hulett, R. Sheahan, B.J. Hathaway, J. Chem. Soc., Dalton Trans. 7 (1981) 1463–1469.
[32] J.K. Walker, R. Nakon, Inorg. Chim. Acta. 55 (1981) 135–140.
[33] M. Duggan, N. Ray, B. Hathaway, G. Tomlinson, P. Brint, K. Pelin, J. Chem. Soc., Dalton Trans. 8 (1980) 1342–1348.
[34] J.G. Gilbert, A.W. Addison, A.Y. Nazarenko, R.J. Butcher, Inorg. Chim. Acta. 324 (2001) 123–130.
[35] A.M. Dittler-Klingemann, C. Orvig, F.E. Hahn, F. Thaler, C.D. Hubbard, R. van Eldik, S. Schindler, I. Fabian, Inorg. Chem. 35 (1996) 7798–7803.
[36] D. Kivelson, R. Neiman, J. Chem. Phys. 35 (1961) 149.
[37] D. Getz, B.L. Silver, J. Chem. Phys. 61 (1974) 630–637.
[38] S. Muthuramalingam, T. Khamrang, M. Velusamy, R. Mayilmurugan, Dalton Trans. 46 (2017) 16065–16076.
[39] B. J. Hathaway, G. Wilkinson, R. D. Gillard, J. A. McCleverty. (Eds.), Comprehensive Coordination Chemistry, Pergamon, Oxford, 5; 1987.
[40] P.F. Rapheal, E. Manoj, M.R. Prathapachandra Kurup, Polyhedron 26 (2007) 818–828.
[41] B.J. Hathaway, A.A.G. Tomlinson, Coord. Chem. Rev. 5 (1970) 1–43.
[42] E.I. Solomon, Inorg. Chem. 45 (2006) 8012–8025.
[43] Q. Zhu, Y. Lian, S. Thyagarajan, S.E. Rokita, K.D. Karlin, N.V. Blough, J. Am. Chem. Soc. 130 (2008) 6304–6305.
[44] (a) A. Rockenbauer, J. Magn. Reson. 35 pp. 429–438; 1979. (b) S. L. Reddy, T. Endo, G. S. Reddy, Electronic (Absorption) Spectra of 3d Transition Metal Complexes. Advanced Aspects of Spectroscopy.
[45] (a) S.V. Kryatov, S. Taktak, I.V. Korendovych, E.V. Rybak-Akimova, Inorg. Chem. 44 (2005) 85–99;
(b) J.A. Halfen, J.M. Uhan, D.C. Fox, M.P. Mehn Jr., L. Que, Inorg. Chem. 39 (2000) 4913–4920;
(c) D. Lee, S.J. Lippard, Inorg. Chem. 41 (2002) 2704–2719;
(d) M. Velusamy, R. Mayilmurugan, M. Palaniandavar, Inorg. Chem. 43 (2004) 6284–6293.
[46] (a) M.S. Balula, J.A. Gamelas, H.M. Carapuc, A.M.V. Cavaleiro, W. Schlindwein, Eur. J. Inorg. Chem. (2004) 619–628;
(b) H.H. Thorp, Encyclopedia of Inorganic and Bioinorganic, Chemistry, John Wiley & Sons, Ltd., 2011;
(c) P. Lemoine, Coord. Chem. Rev. 47 (1982) 55–88.
[47] P. Chen, K. Fujisawa, E.I. Solomon, J. Am. Chem. Soc. 122 (2000) 10177–10193.
[48] (a) S. Kundu, E. Matito, S. Walleck, F.F. Pfaff, F. Heims, B. Rabay, J.M. Luis, A. Company, B. Braun, T. Glaser, K. Ray, Chem. Eur. J. 10 (2012) 2787;
(b) J.D. Parham, G.B. Wijeratne, D.B. Rice, T.A. Jackson, Inorg. Chem. 57 (2018) 2489–2502;
(c) M.S. Reynolds, A. Butler, Inorg. Chem. 35 (1996) 2378–2383;
(d) M.K. Coggins, J.A. Kovacs, J. Am. Chem. Soc. 133 (2011) 12470–12473;
(e) M.K. Coggins, V.M. Diaconescu, S.D. Beer, J.A. Kovacs, J. Am. Chem. Soc. 135 (2013) 4260–4272.
[49] Q. Xing, H. Lv, C. Xia, F. Li, Chem. Commun. 52 (2016) 489.
[50] K.W. Penfield, R.R. Gay, R.S. Himmelwright, N.C. Eickman, V.A. Norris, H.C. Freeman, E.I. Solomon, J. Am. Chem. Soc. 103 (1981) 4382–4388.
[51] M.J. Frisch, G.W. Trucks, H.B. Schlegel, G.E. Scuseria, M.A. Robb, J.R. Cheeseman, G. Scalmani, V. Barone, B. Mennucci, G.A. Petersson, H. Nakatsuji, M. Caricato, X. Li, H.P. Hratchian, A.F. Izmaylov, J. Bloino, G. Zheng, J.L. Sonnenberg, M. Hada, M. Ehara, K. Toyota, R. Fukuda, J. Hasegawa, M. Ishida, T. Nakajima, Y. Honda, O. Kitao, H. Nakai, T. Vreven, J.A. Montgomery Jr, J.E. Peralta, F. Ogliaro, M.J. Bearpark, J. Heyd, E.N. Brothers, K.N. Kudin, V.N. Staroverov, R. Kobayashi, J. Normand, K. Raghavachari, A.P. Rendell, J.C. Burant, S.S. Iyengar, J. Tomasi, M. Cossi, N. Rega, N.J. Millam, M. Klene, J.E. Knox, J.B. Cross, V. Bakken, C. Adamo, J. Jaramillo, R. Gomperts, R.E. Stratmann, O. Yazyev, A.J. Austin, R. Cammi, C. Pomelli, J.W. Ochterski, R.L. Martin, K. Morokuma, V.G. Zakrzewski, G.A. Voth, P. Salvador, J.J. Dannenberg, S. Dapprich, A.D. Daniels, O. Farkas, J.B. Foresman, J.V. Ortiz, J. Cioslowski, D.J. Fox, Gaussian 09 (2009).
[52] G. A. Zhurko, Chemcraft – graphical program for visualization of quantum chemistry computations. Ivanovo, Russia. https://chemcraftprog.com.